Evolution of aerial spider webs coincided with repeated structural optimization of silk anchorages

(Article begins on next page)

28 April 2024

Evolution of aerial spider webs coincided with repeated structural optimization of silk anchorages

Jonas O. Wolff[1]*, Gustavo B. Paterno[1,2], Daniele Liprandi[3], Martín J. Ramírez[4], Federico Bosia[3], Arie van der Meijden[5], Peter Michalik[6], Helen M. Smith[7], Braxton Jones[1], Alexandra M. Ravelo[2], Nicola Pugno[8,9,10], and Marie E. Herberstein[1]

[1] Department of Biological Sciences, Macquarie University, Sydney, NSW 2109, Australia

[2] Instituto de Ciências Biológicas, Programa de Pós-Graduação em Ecologia, Universidade Federal de Juiz de Fora, Rua José Lourenço Kelmer, 36036-900, Juiz de Fora, MG, Brazil.

[3] Department of Physics and Nanostructured Interfaces and Surfaces Interdepartmental Centre, Università di Torino, Via P. Giuria 1, 10125 Torino, Italy

[4] Museo Argentino de Ciencias Naturales "Bernardino Rivadavia", Consejo Nacional de Investigaciones Científicas y Técnicas (CONICET), Av. Ángel Gallardo 470, C1405DJR, Buenos Aires, Argentina

[5] CIBIO Research Centre in Biodiversity and Genetic Resources, InBIO, Universidade do Porto, Campus Agrário de Vairão, Rua Padre Armando Quintas, 4485-661 Vairão, Vila do Conde, Portugal

[6] Zoologisches Institut und Museum, Universität Greifswald, Loitzer Str. 26, 17489, Greifswald, Germany

[7] Australian Museum, 1 William St, Sydney, New South Wales, 2010, Australia

[8] Laboratory of Bio-Inspired and Graphene Nanomechanics, Department of Civil, Environmental and Mechanical Engineering, University of Trento, Via Masiano 77, I-38123 Trento, Italy

[9] School of Engineering and Materials Science, Queen Mary University, Mile End Rd, London E1 4NS, UK

[10] KET Labs, Edoardo Amaldi Foundation, Italian Space Agency, Via del Politecnico snc, 00133 Rome, Italy

* corresponding author: jonas.wolff@mq.edu.au

45   **Abstract**

46   Physical structures built by animals challenge our understanding of biological processes

47 and inspire the development of smart materials and green architecture. It is thus indispensable

48 to understand the drivers, constraints and dynamics that lead to the emergence and modification

49 of building behaviour. Here, we demonstrate that spider web diversification repeatedly

50 followed strikingly similar evolutionary trajectories, guided by physical constraints. We found

51 that the evolution of suspended webs that intercept flying prey was preceded by small changes

52 in silk anchoring behaviour with considerable effects on the robustness of web attachment. The

53 use of nanofiber based capture threads conflicts with the behavioural enhancement of web

54 attachment, and the repeated loss of this trait has driven the evolution of web anchor structure.

55 These findings show that the evolution of building behaviour may be constrained by major

56 physical traits limiting its role in rapid adaptation to a changing environment.

57

58   **Keywords**

59   animal architecture; macro-evolution; evolutionary biomechanics; extended phenotype;

60 spider silk; bio-inspiration

61

From efficient tunnel networks of ant colonies and strikingly effective thermal control of termite mounds to the aesthetic assembly of bower bird displays and ecosystem-forming beaver dams: the complexity, efficiency and far reaching effects of animal buildings excite and inspire [1] - their study may even drive technical innovation towards a greener future [2]. Our understanding of how building behaviour evolves within an ecological context is limited because animal architectures blur the boundaries of an organism's phenotype [3-5].

Spider webs are flagship examples of animal architectures, and their enormous diversity in shape render them an ideal system in which to unravel the evolutionary dynamics of building behaviour. Hypotheses of spider web evolution have been formulated for more than a hundred years, with a focus on the role of putatively singular events, such as the emergence of distinct building routines, specific silk proteins or viscid silk [6-10]. In contrast, recent[11-13] and controversial [14,15] phylogenomic studies favour a more dynamic scenario, where similar behavioural routines have repeatedly evolved. The core of the controversy is the question whether the evolution of behavioural building routines is dynamic and repeatable or slow and determined by contingent events. The answer to this question goes beyond spider webs: if the evolution of behaviour is less constrained than the evolution of physiological and morphological traits it could facilitate rapid responses to environmental changes, thereby setting the course of evolutionary trajectories [4,16,17].

Here, we approach the inference of spider web evolution from a previously neglected angle: the idea that a robust foundation is the basis for a stable building [1]. It has been proposed that the evolution of tape-like thread anchorages at the base of modern spiders (Araneomorphae) ~300 MYA dramatically changed silk usage: spiders were no longer restricted to spinning substrate-bound sheets, but could produce complex three dimensional structures by spatially arranging single lines [9,18]. Despite this early insight, subsequent work has focussed on the role web geometry and silk proteins in the evolution of webs, neglecting the role of web anchorages.

Since anchor strength underlies global mechanical rules, it is possible to derive parameter estimates for its optimization [19]. We hypothesized that lineages that achieve optimal anchor strength by behavioural means, also achieve web types with greater mechanical integrity. To test this, we quantified silk anchor structure and web types in 105 spider species of 45 families, covering all major clades of the modern spiders. We first built a numerical model to identify the optimum in anchor structure and tested if it matched the adaptive peaks in the macro-evolutionary signal. We then related silk anchor performance to anchor building behaviour and the morphology of the spinning apparatus. Specifically, we tested how the innate

96   spinneret choreography during anchor production affects anchor structure [18], and how the

97   configuration of the spinning apparatus affects the kinematic properties of the system. Finally,

98   we determined the sequence of silk anchor enhancement and aerial web evolution: did aerial

99   web building lead to anchor enhancement, or were enhanced anchors a prerequisite for the

100   evolution of aerial webs?

101

102   **Results**

103   *Physical constraints and optima of silk anchorages*

104   Web anchors resemble microscopic webs, consisting of numerous sub-micron sized glue

105   coated fibres, so-called *piriform silk*. These fibres are combined into a patch-like film, taping

106   the main thread, the *dragline*, onto the substrate. The dragline can be embedded all the way

107   through this film, or be attached centrally only. The attachment position of the dragline greatly

108   affects where and how load is transmitted onto the underlying film. The more central the

109   dragline placement the better the anchor can withstand stress from a variably loaded silk line.

110   Preliminary studies have revealed that this is the most significant determinant of web anchor

111   robustness [20].

112   To identify the optimum of the dragline placement parameter c_d (dragline centrality),

113   we built a numerical model based on the theory of thin film contact mechanics [21], approximating

114   silk anchorages as tape like films. To apply our results to a range of silk properties found in

115   spiders, we repeated simulations for parameters measured in the Tasmanian cave spider

116   (*Hickmania troglodytes*), representing an ancient lineage, and in golden orb web spiders

117   (*Nephila plumipes*), a representative of derived aerial web builders. We found that anchor

118   strength improved if its geometrical structure allowed to maximize the peeling line (total length

119   of the detachment front) before detachment, which occurred in the range $c_d = 0.3$–0.5 mm/mm

120   for typical anchorage parameters (Fig. 1a). The exact optimum within this range depends,

121   amongst others, on the material properties of the silk. For draglines as stiff as the anchor silk

122   (or point-like dragline joints) $c_d = 0.5$ and it decreased with an increase in stiffness difference

123   between dragline and anchor silk. During detachment, the stress concentrations and subsequent

124   delamination front approximated a circular shape that became more elliptical as the peeling

125   angle increased (Fig. 2b). The c_d value determined a delay in the detachment front reaching the

126   anchorage edges (for typical anchorage shapes), leading to an overall increase in robustness.

127   This is in agreement with empirical data on silk anchors of orb web spiders (S2) and up-scaled

128   physical models [20]. Notably, the effect of the pulling angle on anchor resistance was reduced at

129 optimal c_d (Fig. 2c,d). This indicates that the benefit of high c_d is realised in dynamic loading

130 situation, such as in aerial webs.

131

132 *Evolutionary dynamics of spider web traits*

133 Spider webs are diverse in shape and function but for the purpose of our analyses we

134 categorised the web phenotypes into: 'substrate webs', 'aerial webs' and 'webless foragers'

135 (see methods for definition). This reflects a different demand in mechanical stability and

136 ecological impact of the web. Our phylogenetic analyses confirmed that substrate webs are the

137 ancestral state in Araneomorphae. Aerial webs have evolved independently at the basis of

138 Araneoidea, in Uloboridae, Deinopidae, Pholcidae, and within Desidae.

139 Lineages with anchors near the physical optimum of $c_d = 0.3–0.5$ included all aerial web

140 builders that lack a cribellum, the cribellate substrate web building Megadictynidae, and some

141 ecribellate hunting spiders of the Mimetidae, Arkyidae, Thomisidae, Oxyopidae, Trechaleidae,

142 Philodromidae, Salticidae and Toxopidae. We found multiple support for six shifts in the

143 evolutionary regime of c_d: *shift 1* in Pholcidae (posterior probability $pp = 0.494$); *shift 2* in the

144 grate-shaped tapetum clade (excl. Zoropsidae) ($pp = 0.474$); *shift 3* at the basis of Salticidae (pp

145 $= 0.405$); *shift 4* at the basis of Entelegynae ($pp = 370$); *shift 5* at the basis of Araneoidea ($pp =$

146 0.336); and *shift 6* within Desidae (*Cambridgea*) ($pp = 0.309$). Shift 5 and 6 (both aerial web

147 spinners; adaptive optimum $\theta \sim 0.36$ mm/mm), and shifts 1, 2 and 3 (aerial web spinning and

148 hunting spiders; $\theta \sim 0.30$ mm/mm) were convergent, shifting towards similar evolutionary

149 optima (Fig. 3f). Shifts 2, 5 and 6 coincided with cribellum loss and shifts 1 and 5 with the

150 evolution of aerial webs. Notably all supported shifts led towards an elevated adaptive optimum

151 θ. Our data suggest that the evolutionary trend towards an elevated c_d happened stepwise, for

152 instance the exceptional c_d in Araneoidea evolved from an estimated root optimum of $\theta \sim 0.18$

153 mm/mm, with the first shift around 250 MYA towards $\theta \sim 0.24$ mm/mm (shift 4), and the

154 second one around 180 MYA towards $\theta \sim 0.36$ mm/mm (shift 5). The exact location of these

155 shifts differed between *SURFACE* and *bayou* methods, and an additional shift at the basis of

156 Nicodamidoidea+Araneoidea around 200 MYA is possible ($pp = 0.290$; Fig. 2; S4; S5). In

157 Uloboridae and Deinopidae only one step occurred (shift 4), approximately 50 MY prior to

158 aerial web evolution in these families. In Pholcidae the single regime shift (shift 1) coincided

159 with aerial web evolution.

160 We found evidence that the evolution of high c_d values has been constrained by the

161 configuration of the spinning apparatus. Spiders with a spinning plate - the cribellum (the basal

162 state) produced a significantly smaller c_d ($p = 0.009$; S6) and cribellum loss generally led to an

163 increase of c_d (Fig. 3b). Furthermore, c_d correlated with spinning choreography, i.e. the relative

164 height of the spinneret trajectory geometry h_r ($p = 0.004$; S6): h_r is on average 1.6 times larger

165 in ecribellate spiders ($p < 0.001$; S6). These results were highly robust to phylogenetic

166 uncertainty (S6). Notably, the shape of the spinning path did not differ between cribellar and

167 ecribellar spiders ($p_r = 0.214$) (S7). This indicates that it is not the shape of the spinning path,

168 but its orientation and proportions that affect c_d. Our kinematic and morphological studies

169 revealed that the cribellum mechanically constrains the mobility of the anchor producing

170 spinnerets (the anterior lateral spinnerets) by blocking them on the anterior side. As a result,

171 most cribellar spiders spread the spinnerets more laterally, leading to smaller h_r and c_d.

172 To further investigate if the configuration of the spinning apparatus (c) and web building

173 behaviour (w) had an effect on the evolutionary dynamics of c_d, we compared the fit of single

174 and two-regime Brownian Motion (BM) and Ornstein-Uhlenbeck (OU) models. To account for

175 phylogenetic uncertainty, we repeated the analyses across a sample of 100 phylogenetic trees.

176 We found strong support for a scenario, where the evolution of anchor structure was

177 highly dynamic in substrate web builders and hunters, but stabilized around an elevated

178 optimum in aerial web builders. Among all models, OUw models provided the best explanation

179 for the extant variation of c_d ($AICcw$ (OUMVAw) = 0.667 ± 0.339; $AICcw$ (OUMAw) =

180 0.163 ± 0.295; Fig. 3a). Under these models c_d evolved at an increased adaptive optimum with a

181 high adaptive potential in aerial web builders, while c_d of substrate web building and hunting

182 spiders followed a stochastic evolution (i.e. $t^{1/2} \gg T$; Fig. 3b,c). There was support that

183 cribellum loss affected the evolution of c_d (mean $\Delta AICc$ (OUMc-BM1) = 3.43, mean $\Delta AICc$

184 (OUMc-OU1) = 4.34). The best fit among OUc-models was the OUMc, a model under which

185 c_d of ecribellar spiders had a higher adaptive optimum θ but evolutionary rates σ^2 and adaptive

186 potential α did not differ between cribellar and ecribellar spiders. The inferred mean $t^{1/2}$ was

187 close to the total height of the tree T, which represents a moderate α [22].

188 Similar analyses on the spinning track proportions h_r indicated five shifts in the

189 evolutionary regime: *shift 1* within Desidae (*Cambridgea*) ($pp = 0.507$); *shift 2* at the basis of

190 Hersiliidae ($pp = 0.584$); *shift 3* at the basis of Araneoidea ($pp = 0.579$); *shift 4* in the grate-

191 shaped tapetum clade (excl. Zoropsidae) ($pp = 0.590$); and shift 5 in Pholcidae ($pp = 0.470$)

192 (Fig. 2). All but shift 5 coincided with cribellum loss, and shifts 1, 3 and 5 co-occurred with

193 aerial webs. Branches accommodating shifts 1, 3, 4 and 5 also had shifts in c_d, indicating a

194 causal link. The constitution of the spinning apparatus had clearly affected the evolution of h_r

195 ($AICcw$(OUMAc) = 0.442 ± 0.247; $AICcw$(OUMVAc) = 0.388 ± 0.269), whereas OUw models

196 were indistinguishable from BM models (Fig. 3d). The contrasting results for c_d indicate that h_r

197 alone does not explain c_d. There is, at least, one additional behavioural component affecting c_d,

198 which is the movement of the body while a series of alternating spinneret movements are

199 performed. The highest c_d values (excluding the hunting spider *Australomisidia*) were found in

200 spiders that perform a back-and-forth movement of the abdomen during anchor production.

201 This behaviour has evolved independently in the Araneoidea and in *Cambridgea*.

202

203

204 **Discussion**

205 This study is the first to assess attachment as a driving component in the evolution of

206 animal architectures. We have shown that small changes in anchor structure profoundly affect

207 web attachment. Notably, structural optimization does not necessarily come at a higher material

208 cost, as the effect of dragline placement is significant for similar sized silk films. It therefore

209 appears counter-intuitive that not all extant spiders exhibit an optimized anchor structure and

210 that anchor building behaviour evolved slowly and stepwise. We found this is due to two

211 reasons: first, the evolution of anchor structure is relaxed in substrate web builders and

212 wandering spiders that do not rely on robust silk anchorages, and second, the evolution of

213 anchor building behaviour is constrained by physical traits.

214 Our data suggests that the cribellum organ, a sophisticated spinning plate that produces

215 nanofiber-based capture threads, is one example of such a physical constraint on behavioural

216 evolution. This is important since it provides an explanation for an old enigmatic problem in

217 the understanding of spider web evolution: why nano-fibre capture silk was lost so frequently

218 across the spider tree, resulting in cribellar spiders being largely outnumbered by ecribellar

219 spiders, and why only few cribellar spiders evolved aerial webs, even though cribellar silk can

220 be highly efficient in prey capture [23-25]. Our results indicate that the cribellum represents a

221 significant constraint on the evolution of robust anchorages limiting the capability to build

222 efficient suspended webs.

223 We found that all changes in the evolutionary mode of anchor spinning behaviour

224 followed or co-occurred with the loss of the cribellum. However, cribellum loss did not lead to

225 changes in the evolutionary dynamics of spinning behaviour *per se*, indicating that further

226 changes of physical traits, such as the arrangement of muscles and spinneret articulation, might

227 have been necessary to alter spinning behaviour in a way to optimize anchor structure.

228 Cribellum loss was thus an important pre-condition for further evolutionary enhancement of

229 silk attachment.

230   Multiple support for an exceptional (i.e. faster and more stabilized) evolution of anchor

231   structure in aerial web builders underlines its adaptive value for such webs. Aerial webs

232   repeatedly evolved after evolutionary shifts in silk anchor structure and anchor spinning

233   behaviour occurred supporting the idea that web anchor performance mediates the evolution of

234   web architecture.

235   Limited anchor performance may thus in itself be an important constraint in the

236   evolution of web building behaviour, and its improvement may have accelerated spider web

237   diversification: web architecture is phylogenetically labile and enormously variable in

238   ecribellate orb-web and cobweb spiders [26-28], lineages in which anchor structure has reached

239   the physical optimum. Such a rapid turnover of web building behaviour may mask evolutionary

240   histories in these lineages. Concluding that similarities in building routines indicate a common

241   origin can be problematic in these cases, since the probability of parallelism is high [16,29]. Our

242   example shows that to understand the evolution of complex behaviour, like orb-web building,

243   it is essential to identify the interdependencies of behavioural and physical traits.

244   We conclude that the evolution of behaviour and extended phenotypes is not as free as

245   previously suggested [4,30-32], but may be tightly bound to evolutionary changes in physical traits.

246   In the case of spider webs the evolutionary removal of such constraints has led to an

247   evolutionary cascade resulting in an enormous diversity of web architectures and outstanding

248   ecological success.

249

250

251   **Material and Methods**

252   *Material sourcing and fieldwork*

253   Spiders were collected in Eastern Australia (NSW, QLD, VIC and TAS), New Zealand (North Island),

254   Germany, Italy, the U.S.A., Argentina and Morocco, or obtained from lab stocks (3 species) and kept in the lab in

255   plastic jars or boxes with slightly moistened tissue (complete list of species and collection data in Tab. S8). We

256   aimed for three individuals per species, while we did not expect differences in our target traits between sexes and

257   developmental stages (confirmed by intraspecific comparison of anchor structure in *Argiope keyserlingi* and

258   *Nephila plumipes*, unpub.). However, for some species only single individuals could be obtained (samples sizes

259   are given in Tab. S1 and Fig. 2). Silk samples were collected on glass slides that were left in the enclosures for 2-

260   7 days. Silk samples were stored in dry boxes and are deposited at the Department of Biological Sciences,

261   Macquarie University (MQ). Voucher specimens of spiders are deposited at the Australian Museum (AM), the

262   Zoological Museum of the University of Greifswald (UG), the Natural History Museum of Argentina (MA),

263   Canterbury Museum (CM) and private collections (see Tab. S8 for details).

264   For each species we recorded the web type based on field and lab observations: 0, no web (hunting spider);

265   1, substrate bound web (capture area ± parallel and directly attached to the substrate surface); 2, aerial web (capture

266   area suspended, indirectly attached to substrate, and its shape ± independent of substrate topography). These

267   categories were chosen, because they represent different demands of a robust anchorage.

268

269   *Morphology of spinning apparatus*

270   Spiders were investigated under dissection microscopes to score two states of the spinning apparatus: 0,

271   ecribellar; 1, cribellar.

272

273   *Kinematics of spinning apparatus*

274   Spinning choreography was studied in a subset of 71 species following the methods described in [20], using

275   a Basler Ace 640×480pix USB 3.0 high speed video camera (Basler AG, Ahrensburg, Germany), equipped with a

276   Navitar Precise Eye extension tube including a 1.33× magnification lens (Navitar, Inc., Rochester, NY, USA). A

277   0.25× accessory lens was used for larger spiders (body length >10 mm). The resulting field of view was 1.3×1.0

278   mm at a pixel size of 2.1 µm for the basic configuration, and 5.3×4.0 mm at a pixel size of 8.3 µm for the

279   configuration with the 0.25× lens. Videos were recorded with 500 frames per second, using the *TroublePix*

280   software (NorPix, Inc., Montreal, QC, Canada) with continuous looping and post event trigger.

281   Videos were processed with *ImageJ 1.5* [33] as detailed in [20]. The movements of both anterior lateral

282   spinnerets were manually tracked using the *MTrackJ* plugin [34], taking the centre of the piriform spigot field on the

283   anterior lateral spinneret apex as a reference. Each spinning sequence consists of a set of stereotypic spinneret

284   trajectories. Single trajectories were extracted, their tracking coordinates positioned in a generalized grid and

285   partitioned into 50 landmarks defined by regularly spaced time intervals (for details on this procedure we refer to

286   [18,20]). This procedure ensures that the relative orientation of the kinematic track shapes towards the animal's body

287   axis is maintained. From these shapes we calculated the relative track proportions h_r as the *y*-dimension divided

288   by the *x*-dimension of the aligned track shape, where the minimal *x*-coordinate denotes the proximal turning point

289   of the adducted spinneret (where the dragline is usually placed) and the maximal *x*-coordinate the lateral turning

290   point of the abducted spinneret. This variable reflects under which angle piriform silk is spread away from the

291   dragline joint.

292   The final dragline location may not only be determined by the trajectories of single kinematic elements,

293   but also how these are applied along the animal's body axis. Some spiders perform a back-and-forth movement of

294   the abdomen to further modulate dragline placement. This behaviour was recorded as a binary character: 0, absent;

295   1, present.

296

297   *Structure and morphometrics of silk anchors*

298   Nine to twenty silk anchors per individual spider were imaged with Leica M205A (Leica Microsystems

299   GmbH, Wetzlar, Germany) and Motic (Motic Inc. Ltd., Hong Kong) stereo microscopes with mounted cameras.

300   Morphometrics of silk anchors was performed on micrographs in *ImageJ*. We calculated the dragline

301   placement variable c_d as follows: distance *d* between the dragline joint (point were the dragline leaves the anchor)

302   and the anterior border of the anchor divided by the longitudinal dimension of the anchor. In anchors of some basal

303   species the individual dragline fibres do not leave the anchor as a bundle, but separately in different locations. In

304   these cases the pair of fibres located closest to the frontal border of the anchor was taken into consideration and

305   their *d*-values were averaged. Details on the morphometric characterization of silk anchors are described in [20].

306

307   *Numerical model*

308   The elastic membrane was modelled by discretising it in a network of elastic bonds (i.e. springs) in a

309   square-diagonal lattice, using a generalized non-linear 3D co-rotational truss formulation [35]. A homogenization

310   procedure was adopted, imposing the equivalence of the strain energy density of the lattice with that of a

311   corresponding homogeneous membrane [36,37]. We used a standardized anchor geometry with length $l = 1$ mm, width

312     $w = 1$ mm, thickness $t = 1$ μm, and with the dragline fused with the membrane over a length of $c_l = 0.33$ mm. To

313   account for differences in silk properties, we performed separate simulations for a combination of membrane and

314   dragline stiffness values, as empirically observed in the basal sheet web spider *H. troglodytes* and the aerial web

315   builder *N. plumipes*: Young's modulus of piriform silk membrane $E_p = 0.25$ GPa for *Hickmania* and $E_p = 1.7$ GPa

316   for *Nephila* (see tensile test methodologies and results in S1), and Young's modulus of dragline $E_d = 10$ GPa for

317   *Hickmania* and $E_d = 15$ GPa for *Nephila* (after [38] and [39]).

318   The interface was modelled assuming a 3D exponential-like traction-separation law (cohesive zone

319   model) of the form $T_i = \Delta_i \frac{\phi_i}{\delta_i^2} \cdot \exp\left(\sum_j -\frac{\Delta_j^2}{\delta_j^2}\right)$ where ϕ_i, Δ_i and δ_i are the work of separation, the crack gap value

320   and the characteristic length (i.e. the gap value corresponding to the maximum traction) [40]. The resulting system

321   of coupled non-linear equations in matrix form was solved using an algorithm based on the Newton-Raphson

322   method [41] implemented in C++ and run on the OCCAM HPC cluster at the University of Torino. The adhesive

323   energy of the interface, calculated as the integral of the cohesive law, was taken to be equal to $\phi = 0.5$ MPa·mm.

324   We simulated the maximal pull-off forces for different c_d between 0.0 and 0.5. To further study the effect

325   of c_d on anchor robustness we simulated maximal pull-off forces for different pull-off angles (loading angles)

326   between 15° (± parallel to substrate along spinning direction) and 165° (± parallel to substrate against spinning

327   direction, e.g. dragline flipped over) for a c_d of 0.0, 0.2 and 0.4.

328

329   *Phylogenetic inference*

330   The phylogenetic tree was estimated using three mitochondrial (12S, 16S, COI) and three nuclear (histone

331   H3, 18S, 28S) markers, taken from the study of Wheeler et al. [42] and supplemented with sequences from GenBank

332   (Table S10). The clades obtained as monophyletic in the genomic analyses of Fernández et al. [11] (Araneae), Kallal

333   et al. [43] (Araneidae), Cheng and Piel [44] (oval calamistrum clade), and Maddison et al. [45] (Salticidae) were

334   constrained for monophyly, as a backbone tree. The reason for such constrained analysis is that our six-markers

335   dataset will not have sufficient signal to overturn the results based on hundreds to thousands of markers from the

336   genomic analyses.

337   We lacked sequence data for 58 of the studied species but were able to use sequences from closely related

338   species to obtain a good estimate of phylogenetic placement and branch lengths (Table S9). For an additional set

339   of 20 species we did not have close relatives, or a close relative was already in the dataset; these were connected

340   randomly in internal branches according to their taxonomic placement (Table S9). Two non-araneomorph

341   terminals were added to root the tree, representing the lineages Mesothelae and Mygalomorphae; these were

342   excluded from the comparative analyses.

343   Alignment of sequences was performed with *MAFFT* version 7 online service [46]. Model selection was

344   made with *jModeltest* [47]. Secondary dating of main tree nodes was assigned as mean and 95% HPD taken from

345   Fernández et al. [11] and analysed in *BEAST2* [48] under a relaxed lognormal clock model [49], using the CIPRES Science

346   Gateway [50] for 50 million generations. After a pilot run, GTR models were simplified to HYK to achieve

347 convergence. The 20 species without sequence data were free to connect anywhere along any branch within

348 taxonomically constrained clades; to avoid for very short tip branches, we placed a uniform prior for the clade age,

349 with minimum 2 mya for congeners and 5 mya for higher taxa.

350 To account for the uncertainty of the phylogenetic estimation, we obtained 100 trees randomly drawn

351 from the post-burnin posterior sample of the Bayesian analysis in *BEAST2*. The subsequent comparative analyses

352 are averaged over these 100 trees, and thus incorporate the uncertainty in phylogenetic parameters.

353

354 *Macro-evolutionary framework*

355 We used phylogenetic comparative methods to infer adaptive peaks and constraints and test evolutionary

356 associations of silk anchor structure, spinning apparatus, spinning kinematics and web building behaviour, using

357 multiple packages in the software environment *R*.

358 Ancestral state estimation of spinning apparatus morphology was performed with stochastic character

359 mapping using the *make.simmap* function in *phytools* [51], with 100 repeats using Equal Rates (*ER*), All Rates

360 Different (*ARD*) and customized models. State 1 (cribellum present) was returned in the ancestral node in all cases,

361 but there were two cases of cribellum loss and re-gain under the ER and ARD models. Since this is a highly

362 unlikely scenario (see [52]), we introduced a rate substitution matrix that supressed state 1 to 2 transitions. The

363 returned simmaps were used to locate events of cribellum loss and for *OUwie* analyses. Ancestral state estimation

364 of web type was done with *ace* in *ape* 5.1 [53] using ER and ARD models.

365 To infer evolutionary dynamics of the continuous variables dragline placement c_d and spinning track

366 dimensions h_r we used a multi-step model-selection process. To test if changes in discreet characters led to

367 differential evolutionary dynamics, we fitted different Brownian Motion (*BM*) and generalized Ornstein-

368 Uhlenbeck-based Hansen models (*OU*) using the package *OUwie* 1.50 [54]. We built a set of models for spinning

369 apparatus state (*c*) and web type (*w*, web type was binary discretized for this purpose in aerial web: 0, no; 1, yes)

370 using a randomly drawn simmap of *c*- and *w*-regimes for each of the 100 trees from our sample. We tested a single-

371 regime BM (*BM1*) and OU model (*OU1*), and per regime type each a two-σ^2 (*BMS*) BM model, and OU models

372 with two θ (*OUM*), two θ and two σ^2 (*OUMV*), two θ and two α (*OUMA*), and two θ, two σ^2 and two σ^2 (*OUMVA*).

373 The corrected Akaike information criterion (*AICc*) was used to compare the fit between all 12 models by

374 calculating the *AICc* weight (*AICcw*) for each tree. *AICcw* and model parameters were then summarized across all

375 100 trees and their median and variance assessed to select for the model(s) that could best explain the data. For

376 each c_d and h_r we ran two loops across the tree sample to check for the effect of the stochastic component in this

377 procedure, and found comparable results (i.e. similar models were favoured and no major differences in median

378 parameter estimates).

379 While prior clade assignments are useful to compare defined groups, they may miss some hidden patterns

380 caused by unstudied effects. We therefore additionally used the methods *SURFACE* [55] and *bayou* [56] on the

381 consensus tree (S3). *SURFACE* performs stepwise AIC estimation to identify regime shifts in θ assuming evolution

382 under the OU process with constant σ^2 and α. *bayou* uses a reverse-jump Markov chain Monte Carlo procedure for

383 the similar purpose. By this, we also checked, if evolution of our variables was driven by singular events (i.e. the

384 occurrence of only a single shift), which may bias PGLS inference [57]. Because the results of *bayou* can be sensitive

385 to the mean number of shifts in the prior [56,58], we ran each two chains over 500,000 generations for prior means of

386 10, 15, 20, and 25 shifts with equal shift probability and one shift maximum per branch, discarding the first 30%

387 as burn-in. For c_d chains with priors of 20 and 25 shifts and for h_r chains with priors of 15, 20 and 25 shifts arrived

388   at a similar posterior (S5). Results are reported from these chains only (means of converged chains given, and

389   graphical representation of shifts for c_d from a randomly chosen chain with a prior of 25 shifts and for h_r from a

390   randomly chosen chain with a prior of 20 shifts).

391

392   *Trait correlation*

393   To reveal patterns of trait correlation we used phylogenetic generalized least squares models (PGLS),

394   which accounts for the non-independence of observations due to common evolutionary history [59-61], across

395   pairwise combinations of our variables: (1) c_d ~ *spinning apparatus*; (2) c_d ~ *web type*; (3) h_r ~ *spinning apparatus*;

396   and (4) h_r ~ *web type*. Further, we performed PGLS regressions between c_d ~ h_r. PGLS analyses were performed

397   with the R package *phylolm* [62] and branch length transformation were optimized by setting *lambda* value through

398   maximum likelihood. To account for phylogenetic uncertainty in PGLS results [63] we repeated each model across

399   our posterior sample of 100 phylogenetic trees. The influence of phylogenetic uncertainty on results was estimated

400   by the variation in model parameters across all runs. Phylogenetic sensitivity analyses were performed for each

401   PGLS model with the R package *sensiPhy* [64].

402

403   *Geometric Morphometrics*

404   To test if the shape of spinning paths differed between spiders with different spinning apparatus and web

405   type, and if it correlates with c_d and h_r, geometric morphometrics was performed using the R package *geomorph*

406   [65]. For this purpose aligned spinneret trajectories were discretized into 50 landmarks with similar time steps, as

407   described in [18]. We used both an alignment towards the median axis between the paired spinnerets which keeps

408   the angular orientation of the trajectories (see [18]), and General Procrustes Alignment (GPA), which omits this

409   information and extracts the pure shape. We then performed Phylogenetic Procrustes ANOVA against the variable

410   'spinning apparatus' and 'web type' and Phylogenetic Procrustes Regression against variables c_d and h_r using the

411   consensus tree.

412

413

436

437 **Author contributions**

438 JOW devised, led and administered the project. JOW, BJ, AMR and PM collected the data. MJR
439 performed the phylogenetic inference. GBP, JOW and AvdM performed the phylogenetic comparative analysis.
440 NMP and FB developed and supervised, and DL carried out the physical numerical simulations. H.S. and M.J.R.
441 ensured taxonomic integrity. JOW, FB and MEH wrote the manuscript. All authors critically revised the
442 manuscript and approved its final version. M.E.H. and N.M.P. mentored the project.

443

444 **Competing Interests**

445 The authors declare that they have no conflict of interests.

446

447 **Data accessibility**

448 Data matrices, trees, R code and additional details of statistical results are deposited in the electronic
449 supplemental material of this paper.

450

451 **References**

452 1   Hansell, M. H. *Animal architecture.* (Oxford University Press, 2005).
453 2   Turner, J. S. & Soar, R. C. in *First International Conference on Industrialized, Intelligent Construction*
454   *at Loughborough University.* (eds I. Wallis, L. Bilan, M. Smith, & A. S. Kaz).
455 3   Dawkins, R.   (Oxford: Oxford University Press, 1982).
456 4   Odling-Smee, F. J., Odling-Smee, H., Laland, K. N., Feldman, M. W. & Feldman, F. *Niche construction:*
457   *the neglected process in evolution.* (Princeton university press, 2003).
458 5   Bailey, N. W. Evolutionary models of extended phenotypes. *Trends Ecol Evol* **27**, 561-569 (2012).
459 6   Eberhard, W. G. Function and phylogeny of spider webs. *Annual review of Ecology and Systematics* **21**,
460   341-372 (1990).
461 7   Blackledge, T. A. *et al.* Reconstructing web evolution and spider diversification in the molecular era.
462   *Proceedings of the National Academy of Sciences* **106**, 5229-5234 (2009).
463 8   Bond, J. E. & Opell, B. D. Testing adaptive radiation and key innovation hypotheses in spiders. *Evolution*
464   **52**, 403-414 (1998).
465 9   Coddington, J. A. in *Spiders of North America: an identification manual.* (eds D Ubick, P Paquin, P.E.
466   Cushing, & V. Roth) 18-24 (American Arachnological Society, 2005).
467 10   Coddington, J. A. in *Spiders. Webs, Behavior, and Evolution* (ed W.A Shear) 319-363 (Stanford
468   University Press, 1986).
469 11   Fernández, R. *et al.* Phylogenomics, diversification dynamics, and comparative transcriptomics across
470   the spider tree of life. *Curr Biol* **28**, 1489-1497 (2018).
471 12   Bond, J. E. *et al.* Phylogenomics resolves a spider backbone phylogeny and rejects a prevailing paradigm
472   for orb web evolution. *Curr Biol* **24**, 1765-1771 (2014).
473 13   Fernández, R., Hormiga, G. & Giribet, G. Phylogenomic analysis of spiders reveals nonmonophyly of
474   orb weavers. *Curr Biol* **24**, 1772-1777 (2014).
475 14   Garrison, N. L. *et al.* Spider phylogenomics: untangling the Spider Tree of Life. *PeerJ* **4**, e1719 (2016).
476 15   Eberhard, W. G. Modular patterns in behavioural evolution: webs derived from orbs. *Behaviour* **155**, 531-
477   566 (2018).

478 16 Ord, T. J. & Summers, T. C. Repeated evolution and the impact of evolutionary history on adaptation.
479   *Bmc Evol Biol* **15**, 137 (2015).
480 17 Wcislo, W. T. Behavioral environments and evolutionary change. *Annual Review of Ecology and*
481   *Systematics* **20**, 137-169 (1989).
482 18 Wolff, J. O., van der Meijden, A. & Herberstein, M. E. Distinct spinning patterns gain differentiated
483   loading tolerance of silk thread anchorages in spiders with different ecology. *Proceedings of the Royal*
484   *Society B: Biological Sciences* **284**, 20171124 (2017).
485 19 Pugno, N. M., Cranford, S. W. & Buehler, M. J. Synergetic material and structure optimization yields
486   robust spider web anchorages. *Small* **9**, 2747-2756, doi:DOI 10.1002/smll.201201343 (2013).
487 20 Wolff, J. O. & Herberstein, M. E. 3D-printing spiders: back-and-forth glue application yields silk
488   anchorages with high pull-off resistance under varying loading situations. *J R Soc Interface* **14**, 20160783
489   (2017).
490 21 Pugno, N. M. The theory of multiple peeling. *Int J Fracture* **171**, 185-193 (2011).
491 22 Cooper, N., Thomas, G. H., Venditti, C., Meade, A. & Freckleton, R. P. A cautionary note on the use of
492   Ornstein Uhlenbeck models in macroevolutionary studies. *Biol J Linn Soc* **118**, 64–77 (2016).
493 23 Bott, R. A., Baumgartner, W., Bräunig, P., Menzel, F. & Joel, A.-C. Adhesion enhancement of cribellate
494   capture threads by epicuticular waxes of the insect prey sheds new light on spider web evolution. *Proc.*
495   *R. Soc. B* **284**, 20170363 (2017).
496 24 Opell, B. D. & Schwend, H. S. Adhesive efficiency of spider prey capture threads. *Zoology* **112**, 16-26
497   (2009).
498 25 Opell, B. The ability of spider cribellar prey capture thread to hold insects with different surface features.
499   *Funct Ecol*, 145-150 (1994).
500 26 Blackledge, T. A. & Gillespie, R. G. Convergent evolution of behavior in an adaptive radiation of
501   Hawaiian web-building spiders. *Proceedings of the National Academy of Sciences* **101**, 16228-16233
502   (2004).
503 27 Kuntner, M., Kralj-Fišer, S. & Gregorič, M. Ladder webs in orb-web spiders: ontogenetic and
504   evolutionary patterns in Nephilidae. *Biol J Linn Soc* **99**, 849-866 (2010).
505 28 Eberhard, W. G., Agnarsson, I. & Levi, H. W. Web forms and the phylogeny of theridiid spiders (Araneae:
506   Theridiidae): chaos from order. *Systematics and biodiversity* **6**, 415 (2008).
507 29 York, R. A. & Fernald, R. D. The Repeated Evolution of Behavior. *Frontiers in Ecology and Evolution*
508   **4**, 143 (2017).
509 30 West-Eberhard, M. J. Phenotypic plasticity and the origins of diversity. *Annual review of Ecology and*
510   *Systematics* **20**, 249-278 (1989).
511 31 Bailey, N. W., Marie-Orleach, L. & Moore, A. J. Indirect genetic effects in behavioral ecology: does
512   behavior play a special role in evolution? *Behav Ecol* **29**, 1-11 (2018).
513 32 Duckworth, R. A. The role of behavior in evolution: a search for mechanism. *Evolutionary ecology* **23**,
514   513-531 (2009).
515 33 Schneider, C. A., Rasband, W. S. & Eliceiri, K. W. NIH Image to ImageJ: 25 years of image analysis.
516   *Nat methods* **9**, 671-675 (2012).
517 34 Meijering, E., Dzyubachyk, O. & Smal, I. Methods for Cell and Particle Tracking. *Methods in*
518   *Enzymology* **504**, 183-200 (2012).
519 35 Cook, R. D., Malkus, D. S. & Plesha, M. E. *Concepts and applications of finite element analysis*. (John
520   Wiley & Sons, 2001).
521 36 Ostoja-Starzewski, M. Lattice models in micromechanics. *Applied Mechanics Reviews* **55**, 35-60 (2002).
522 37 Brely, L., Bosia, F. & Pugno, N. M. A hierarchical lattice spring model to simulate the mechanics of 2-D
523   materials-based composites. *Frontiers in Materials* **2**, 51 (2015).
524 38 Piorkowski, D. *et al.* Ontogenetic shift toward stronger, tougher silk of a web-building, cave-dwelling
525   spider. *J Zool* **304**, 81-89 (2018).
526 39 Swanson, B., Blackledge, T., Beltrán, J. & Hayashi, C. Variation in the material properties of spider
527   dragline silk across species. *Applied Physics A* **82**, 213-218 (2006).
528 40 Salehani, M. K. & Irani, N. A coupled mixed-mode cohesive zone model: An extension to three-
529   dimensional contact problems. *arXiv preprint arXiv:1801.03430* (2018).
530 41 Ostrowski, A. M. in *Third Edition of Solution of Equations and Systems of Equations* Vol. 9 *Pure and*
531   *Applied Mathematics* (ed A.M. Ostrowski) 53-55 (Elsevier, 1973).
532 42 Wheeler, W. C. *et al.* The spider tree of life: phylogeny of Araneae based on target-gene analyses from
533   an extensive taxon sampling. *Cladistics* **33**, 574-616 (2017).
534 43 Kallal, R. J., Fernández, R., Giribet, G. & Hormiga, G. A phylotranscriptomic backbone of the orb-
535   weaving spider family Araneidae (Arachnida, Araneae) supported by multiple methodological
536   approaches. *Mol Phylogenet Evol* **126**, 129-140 (2018).
537 44 Cheng, D.-Q. & Piel, W. H. The origins of the Psechridae: Web-building lycosoid spiders. *Mol*
538   *Phylogenet Evol* **125**, 213-219 (2018).

539 45 Maddison, W. P. *et al.* A genome-wide phylogeny of jumping spiders (Araneae, Salticidae), using
540   anchored hybrid enrichment. *Zookeys*, 89 (2017).
541 46 Katoh, K., Rozewicki, J. & Yamada, K. D. MAFFT online service: multiple sequence alignment,
542   interactive sequence choice and visualization. *Briefings in bioinformatics* (2017).
543 47 Darriba, D., Taboada, G. L., Doallo, R. & Posada, D. jModelTest 2: more models, new heuristics and
544   parallel computing. *Nature methods* **9**, 772 (2012).
545 48 Bouckaert, R. *et al.* BEAST 2: a software platform for Bayesian evolutionary analysis. *Plos Comput Biol*
546   **10**, e1003537 (2014).
547 49 Drummond, A. J., Ho, S. Y., Phillips, M. J. & Rambaut, A. Relaxed phylogenetics and dating with
548   confidence. *PLoS biology* **4**, e88 (2006).
549 50 Miller, M. A., Pfeiffer, W. & Schwartz, T. in *Gateway Computing Environments Workshop (GCE), 2010.*
550   1-8 (Ieee).
551 51 Revell, L. J. phytools: an R package for phylogenetic comparative biology (and other things). *Methods
552   in Ecology and Evolution* **3**, 217-223 (2012).
553 52 Miller, J. A. *et al.* Phylogenetic affinities of the enigmatic spider family Penestomidae (new rank), generic
554   phylogeny of Eresidae, and other advances in spider phylogeny (Araneae, Araneoidea, Entelegynae). *Mol
555   Phylogenet Evol* **55**, 786–804 (2010).
556 53 Paradis, E., Claude, J. & Strimmer, K. APE: analyses of phylogenetics and evolution in R language.
557   *Bioinformatics* **20**, 289-290 (2004).
558 54 Beaulieu, J. & O'Meara, B. OUwie: analysis of evolutionary rates in an OU framework. *R package
559   version* **1** (2014).
560 55 Ingram, T. & Mahler, D. L. SURFACE: detecting convergent evolution from comparative data by fitting
561   Ornstein-Uhlenbeck models with stepwise Akaike Information Criterion. *Methods in Ecology and
562   Evolution* **4**, 416-425 (2013).
563 56 Uyeda, J. C. & Harmon, L. J. A novel Bayesian method for inferring and interpreting the dynamics of
564   adaptive landscapes from phylogenetic comparative data. *Systematic biology* **63**, 902-918 (2014).
565 57 Uyeda, J. C., Zenil-Ferguson, R. & Pennell, M. W. Rethinking phylogenetic comparative methods.
566   *Systematic Biology*, syy031 (2018).
567 58 Ho, L. S. T. & Ané, C. Intrinsic inference difficulties for trait evolution with Ornstein-Uhlenbeck models.
568   *Methods in Ecology and Evolution* **5**, 1133-1146 (2014).
569 59 Felsenstein, J. Phylogenies and the comparative method. *The American Naturalist* **125**, 1-15 (1985).
570 60 Grafen, A. The phylogenetic regression. *Phil. Trans. R. Soc. Lond. B* **326**, 119-157 (1989).
571 61 Freckleton, R. P., Harvey, P. H. & Pagel, M. Phylogenetic analysis and comparative data: a test and
572   review of evidence. *The American Naturalist* **160**, 712-726 (2002).
573 62 Tung Ho, L. s. & Ané, C. A linear-time algorithm for Gaussian and non-Gaussian trait evolution models.
574   *Systematic biology* **63**, 397-408 (2014).
575 63 Donoghue, M. J. & Ackerly, D. D. Phylogenetic uncertainties and sensitivity analyses in comparative
576   biology. *Phil. Trans. R. Soc. Lond. B* **351**, 1241-1249 (1996).
577 64 Paterno, G. B., Penone, C. & Werner, G. D. sensiPhy: An r-package for sensitivity analysis in
578   phylogenetic comparative methods. *Methods in Ecology and Evolution* **9**, 1461-1467 (2018).
579 65 Adams, D. C. & Otárola-Castillo, E. geomorph: an R package for the collection and analysis of geometric
580   morphometric shape data. *Methods in Ecology and Evolution* **4**, 393-399 (2013).
581
582
583

Figure legends

Fig. 1. Optimization of web anchor performance. *(a)* Simulated peak pull-off forces (anchor strength) vs. different dragline positions for silk properties of Tasmanian cave spiders (*H. troglodytes*) and golden orb weavers (*N. plumipes*) under vertical load. The yellow shade indicates the estimated range of c_d (for a variety of silk properties), where anchor strength is maximized. *(b)* Exemplary maps of interfacial stress in the silk membrane (apical view) for an orb weaver silk anchor with $c_d = 0.0$ and $c_d = 0.4$ under vertical load. Warm colours indicate high stress. Anchors reach the peak pull-off force when the interfacial stress concentration around the peeling line reaches the membrane edge. *(c)* Simulated anchor strength for different dragline loading angles between 15° (± parallel to substrate along spinning direction) and 165° (± parallel to substrate against spinning direction, i.e. dragline flipped over) and three different values of c_d (different colours, bold font indicates the mean c_d naturally found in this species) for silk properties of Tasmanian cave spiders. *(d)* Same as in (c) for silk properties of golden orb weavers. Inset shows three-dimensional displacement map and stress distribution in an anchor with $c_d = 0.4$, pulled at an angle of 75° (top-side view).
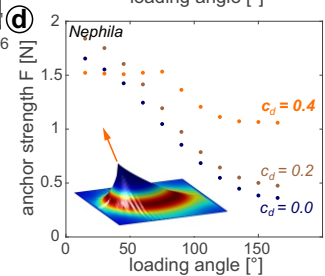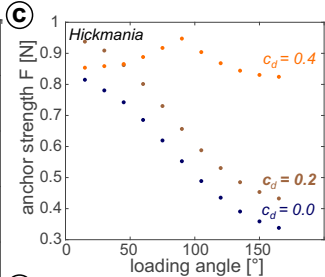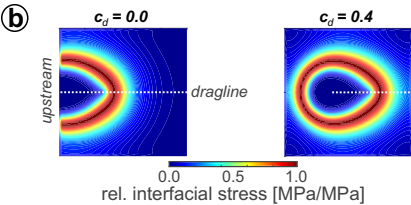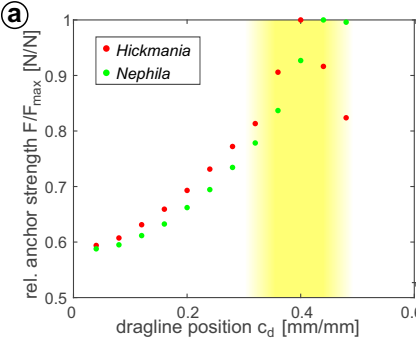
Fig. 2. Correlated evolution of web structure, behaviour and morphology. Shifts in the adaptive landscape of dragline placement c_d (left tree) and spinning choreography h_r (right tree). Branch colours denote convergent evolutionary regimes in the adaptive optimum θ as identified by *SURFACE*, with warmer colours indicating higher θs. The size of overlaid red pies indicates the posterior probability of a shift in θ in that branch, as found by *bayou*. Numbered shifts mark well supported shifts with $pp > 0.3$. White arrowheads with red outline indicate branches in which cribellum loss occurred, and green arrowheads indicate branches in which aerial web building has evolved (with a probability > 0.5). Dots at tips display c_d and h_r values measured in the extant species (grey dots represent means of individuals, black dot species means). The underlying shade indicates web building behaviour (white - no web, red - substrate web, green - aerial web) and the range of optimal anchor structure (yellow shade). Red boxes denote species with a cribellum. Schematics above symbolize anchors with a low and a high c_d (left; top view of anchor with membrane in blue and fused dragline in red) and spinning paths with a low and a high h_r (right; spinneret abducting to the right).
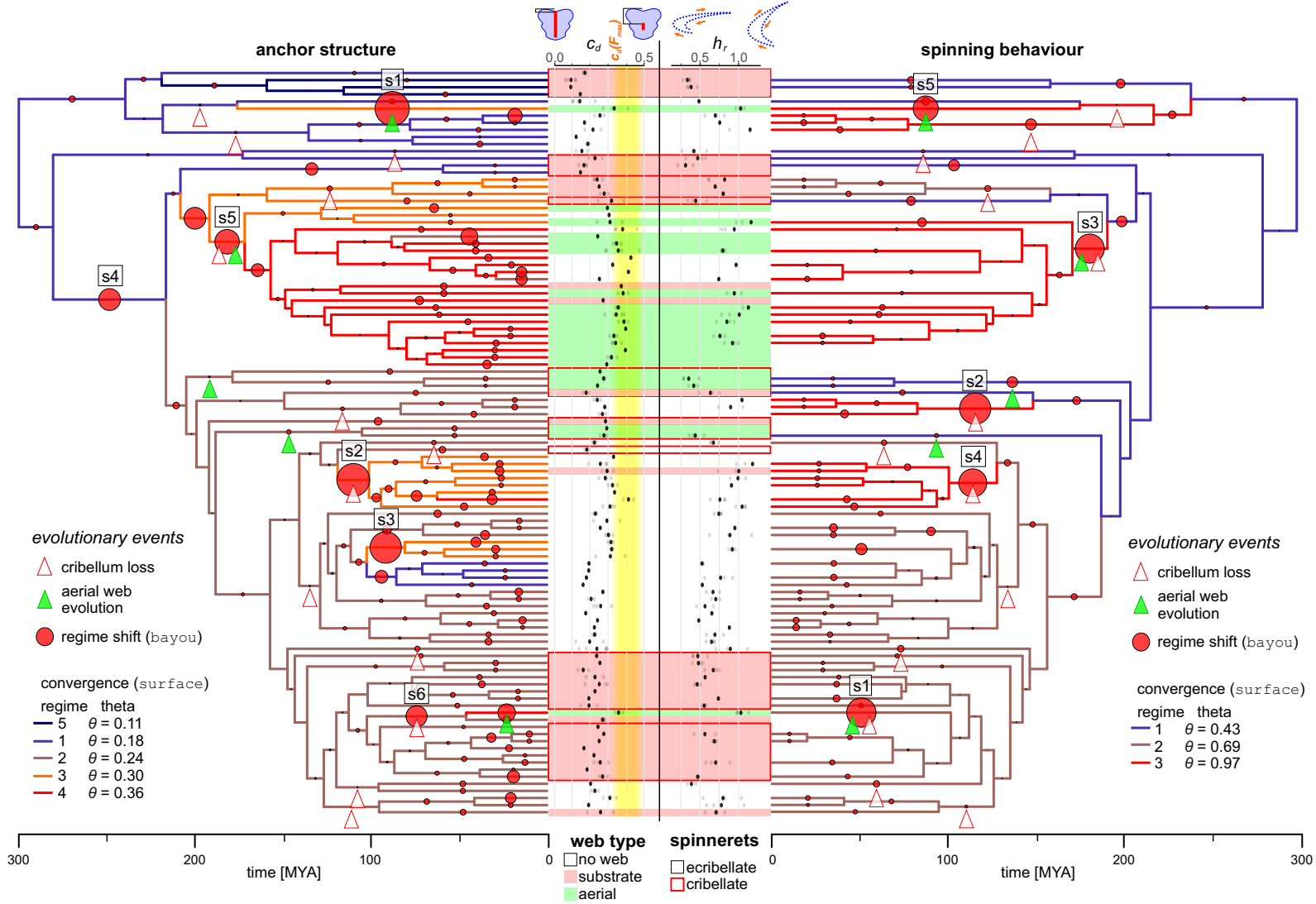
Fig. 3. Exceptional evolution of anchor structure in aerial web builders. *(a)* *AICc*-weight values for single- and two-regime evolutionary models of dragline placement c_d across 100 trees (best supporting model in bold font). A clear support for OUMAw and OUMVAw indicates that c_d evolved towards an elevated optimum and at a higher adaptive potential (and higher evolutionary rates) in aerial web builders. *(b)* Summary of adaptive potential α of c_d for single regime OU-models ('null'-model), and the two regimes of the best fitting OUw model across 100 trees (some extreme outliers not displayed). The black dotted line indicates an α for which the phylogenetic half-life $t^{1/2}$ equals the total tree height T; below this threshold evolution becomes highly labile and BM-like (grey area). *(c)* Summary of the evolutionary optimum θ of c_d for single regime OU-models ('null'-model), and the two regimes of the best fitting OUw models across 100 trees. The yellow area indicates the theoretical physical optimum $c_d(F_{max})$. *(d)* Same as in (a) for spinning choreography h_r. A clear support for OUMAc and OUMVAc indicates that h_r evolved towards an elevated optimum and at a higher adaptive potential (and higher evolutionary rates) after cribellum loss. *(e)* Summary of adaptive potential α of h_r for single regime OU-models ('null'-model), and the two regimes of the best fitting OUc model across 100 trees. Same conventions as in (b). *(f)* Summary of the evolutionary optimum θ of h_r for single regime OU-models ('null'-model), and the two regimes of the best fitting OUc models across 100 trees. Same conventions as in (c).

635
636
Electronic Supplemental Material (*ESM*)

639   **S1.** Estimation of silk membrane stiffness.
640   **S2.** Comparing numerical model results of silk anchor efficiency with empirical data.
641   **S3.** Consensus tree.
642   **S4.** Summary of SURFACE results.
643   **S5.** Summary of bayou results.
644   **S6.** Summary of PGLS results.
645   **S7.** Summary of geometric morphometrics results.
646   **S8.** Material list and sample sizes.
647   **S9.** Terminals mapping.
648   **S10.** Genbank identifiers.
649   **S11.** R code including data and tree files (zipped archive).

(a) rel. anchor strength F/F_{max} [N/N] vs dragline position c_d [mm/mm]
- Hickmania (red)
- Nephila (green)

(b) $c_d = 0.0$ and $c_d = 0.4$; upstream, dragline; rel. interfacial stress [MPa/MPa]

(c) Hickmania: anchor strength F [N] vs loading angle [°]; $c_d = 0.4$, $c_d = 0.2$, $c_d = 0.0$

(d) Nephila: anchor strength F [N] vs loading angle [°]; $c_d = 0.4$, $c_d = 0.2$, $c_d = 0.0$

anchor structure

c_d

c_d / F_{max}

h_r

spinning behaviour

0,0   0,5   0,5   1,0

s1

s5

s4

s5

s3

s2

s5

s2

s4

s3

s2

evolutionary events

△ cribellum loss

▲ aerial web evolution

● regime shift (`bayou`)

convergence (`surface`)

regime	theta
5	$\theta = 0.11$
1	$\theta = 0.18$
2	$\theta = 0.24$
3	$\theta = 0.30$
4	$\theta = 0.36$

s6

s1

evolutionary events

△ cribellum loss

▲ aerial web evolution

● regime shift (`bayou`)

convergence (`surface`)

regime	theta
1	$\theta = 0.43$
2	$\theta = 0.69$
3	$\theta = 0.97$

300   200   100   0

time [MYA]

0   100   200   300

time [MYA]

web type   **spinnerets**

☐ no web   ☐ ecribellate

🟥 substrate   🟥 cribellate

🟩 aerial

a *model support* (`OU`wie)

anchor structure

AICcw

BM1 | OU1 | BMSc | OUMc | OUMVc | OUMAc | OUMVAc | BMSw | OUMw | OUMVw | OUMAw | **OUMVAw**

single regime | spinning apparatus | web type

b *adaptive pull*

α [10^{-2} MY^{-1}]

$t\frac{1}{2} = T$

substrate + no web | aerial

OU1 | OUMVAw

c *optimum*

$c_o(F_{max})$

θ [mm/mm]

substrate + no web | aerial

OU1 | OUMVAw

d

spinning behaviour

AICcw

BM1 | OU1 | BMSc | OUMc | OUMVc | **OUMAc** | **OUMVAc** | BMSw | OUMw | OUMVw | OUMAw | OUMVAw

single regime | spinning apparatus | web type

e

α [10^{-2} MY^{-1}]

$t\frac{1}{2} = T$

cribellar | **ecribellar**

OU1 | OUMAc

f

θ [mm/mm]

cribellar | **ecribellar**

OU1 | OUMAc